23/07/2024 13:12

(Article begins on next page)

Recycling of Yttria stabilized Zirconia waste powders in glazes suitable for ceramic tiles

SCHOLARONE™
Manuscripts

Recycling of Yttria stabilized Zirconia waste powders in glazes suitable for ceramic tiles

C. Siligardi*, S. Barbi*, R. Casini[§], L. Tagliaferri[°], V. Remigio[#]

*Department of Engineering "Enzo ferrari" Via Vivarelli 10/1 41125 Modena, Italy

§ Fritta Italia SrL, GVia della Stazione 31, Fiorano Modenese (MO), Italy

°Turbocoating SpA,Via Mistrali 7, 43040 Rubbiano di Solignano (PR), Italy

Ceramica Fondovalle 12 Via Rio Piodo, 41053 Torre Maina, (MO), Italy

Abstract

The aim of this work is demonstrate the feasibility of valorizing and recycling Yttria stabilized

Zirconia (YSZ) thermal spray waste into high value products for industrial and residential use.

Based on the powders chemistry and morphology, this work aims to realize products, like frits

suitable for white glazes and ceramic tiles. The focus is on one class of powder: high temperature

and abrasion resistant ceramics, like Yttria stabilized zirconia. This study has revealed that the

substitution of pure zirconia with waste Yttria stabilized zirconia is possible in high percentages,

up to 100% to prepare frits suitable for white glazes.

Keywords: waste disposal, glazes, zirconia: yttria stabilized

1. Introduction

Nowadays the recycling and reuse of ceramic materials is even more important not only because

of the environmental issue but also because of the high cost of mining and transport of pure raw

material. In fact this general topic has already been taken into account from a high number of

studies [1]. The present study has the aim to develop in detail the recycling of Yttria stabilized

Zirconia (YSZ) waste powders from thermal barrier coating application to traditional ceramic

tiles.

In particular, considering the commercial frits, suitable for single-fast firing of ceramic tile, those containing zircon ($ZrSiO_4$) and zirconia (ZrO_2) are of great interest, and are commonly named as ''white of zirconium'' [2]. Generally the composition of this category of frits is characterized by 50-60 wt% of SiO_2, 8-14wt% of ZrO_2, 20-25wt% of fluxing elements such as Na_2O, K_2O, and B_2O_3 and 7-9wt% of stabilizing elements such as ZnO, Al_2O_3, CaO, BaO, MgO as minor components [2]. $ZrSiO_4$ was proved to promote opacity, as whitening agent, in presence of ZnO and providing that the SiO_2/Al_2O_3 molar ratio is equal to 10 [3-6]. The mechanism behind the peculiar optical properties of $ZrSiO_4$ is due to the particle size of zircon crystals that approaches the wavelength of incoming light enhancing light scattering and, thus, opacification [7]. $ZrSiO_4$ can be included as ZrO_2 in the frit where the combination with excess silica led to the formation of zircon crystals, that promotes opacification regardless the zirconium compound employed in the glaze formulation [7-8]. The glazes developed from that frits category may have different surface appearance, according with other frits or raw material inside the glazes formulation, such as glossy or opaque. More details about the chemical properties and microstructure of zirconium glazes can be found in previous works [7,9-10]. Moreover, Zircon is generally imported in Europe from Australia or South Africa [11], increasing the cost of this material and contributing to market speculation with an high cost fluctuation [6,11]

Zirconia is a very important industrial ceramic material for structural applications due to its high toughness at high temperature. Zirconia has found use mainly in oxygen pumps and sensors, fuel cells and thermal barrier coatings. However, most engineering applications make use of the tetragonal and cubic phases obtained through the stabilization or partial stabilization of the tetragonal forms, through the introduction of dopants such as Y_2O_3 oxide [12]. Yttria Stabilized Zirconia (YSZ) is one of the most widely used ceramic materials for TBC applications because of

its low thermal conductivity, high-temperature stability in oxidizing and reducing environments, coefficient of thermal expansion similar to Ni/Co based super-alloys, high toughness, and cost-efficiency, by which it can be applied onto metal surfaces. Yttria Stabilized Zirconia (YSZ) can be found in combustor liners, transition sections, nozzle guide vanes, and rotor blades for gas turbine applications [12]. Yttria stabilized zirconia has been established as standard material for the top coat in thermal barrier coating in the last years through thermal spray technology [13-15]. In general the processes consists of injecting a feedstock material (in powder form, seldom as wire) into a hot gas stream generated by a thermal spray torch. The stream heats the powder particles (or melts the wire tip, removing liquid droplets) and drags them towards a target substrate, where they impinge at high temperature and velocity. The coating is therefore built up by the superposition of various layers of flattened particles (often called "lamellae" or "splats") as the torch, usually controlled by an industrial robot, traverses repeatedly in front of the substrate. [16]

Specifically, the TURBOCOATING SpA (Rubbiano di Solignano, Italy) company involved in this research focuses on aeronautics (gas turbine aircraft engines) and energy production (industrial gas turbines) coating applications. Turbocoating applies ceramic coatings, in particular Yttria Stabilized Zirconia (YSZ) for thermal insulation and erosion protection, by atmospheric plasma spraying. In the same spray booths used for ceramic coating also low pressure plasma spraying and high velocity oxygen-fuel spraying are employed to produce Ni- and Co- based alloy coatings (NiCoCrAlY alloys) for oxidation and hot corrosion protection.

In all cases, thermal spray processes run in enclosed environments (spray booths) attached to exhaust systems equipped with dust separation filters. From the environmental point of view, one of the main problems of this technology is that during the spraying process, a significant fraction of the powders is indeed not deposited onto the substrate. Due to the stochastic nature of the

particle injection and treatment inside gas flows, some particles may reach the substrate with inadequate velocity and/or temperature, which results in their rebounding off the target upon impact, without deposition. As a result, a fraction of the feedstock powder usually ranging from 50% up to 80% is not deposited onto the substrate, and it is either collected at the booth floor or inside the dust filters. These spent powders are not re-usable in the thermal spray process itself, because of various reasons. In particular because these spent powders may have been deformed and/or fragmented, so that the shape and size distribution of the spent powder particles is usually altered compared to the original ones, which is unacceptable for a thermal spray process, where a very precisely controlled particle size distribution is needed to maintain the desired coating quality and reproducibility. Moreover, powder contamination may arise from a variety of sources, including wear of the powder feeding and spraying equipment, wear of the exhaust and dust collection system, detachment of debris or fragments from the substrate, etc. The powders that have fallen down in the spraying booth after spraying is collected from the ground or from the air filters and must be treated as waste. Presently, the powders collected in the booth and/or in the dust collection system are treated as "special waste" and, due to the presence of elements such as Ni, Co or other heavy metals (contributed by the powder itself and/or by contaminations), they are labeled as hazardous, which increases the complexity and costs of their disposal and eventual dumping [17].

The aim of this work is to characterize and reuse spent feedstock YSZ powders recovered at the end of various thermal spray processes by TURBOCOATING SpA. In the first part of this study two overspray zirconia powders, coming from two different spray boots, has been characterized in order to analyze particle morphology, size distribution, color, chemical and phase composition. Through these results, the contaminations level introduced by the thermal spray processing has been identified and suitable classification and purification methods have been studied. Different

fraction of the purified powder has been characterized subsequently in order to verify the contamination level obtained after the cleaning process. The best fractions, in terms of chemical purity and homogenous particle morphology and distribution, have been employed to formulate industrial frits suitable for white glazes with a substitution up to 100% of pure zirconia with purified overspray zirconia. These new frits have been compared with an industrial standard frit suitable for white glazes. Subsequently three different glazes has been prepared using the new frits and compared with industrial standard white glaze.

This paper regards the continuous of the study published in 2014 by Siligardi et al. [18] where the substitution of pure zirconia with waste zirconia in a ceramic glaze, was possible only in small percentages due to the presence of chromophore ions into waste zirconia, which tend to color the glaze.

2. Materials and Methods

Two different YSZ overspray waste powders were delivered from Turbocoating SpA. Samples, labeled as Z1AR (Zirconia 1 as received) and Z2AR (Zirconia 2 as received), came from two different spraying booths. Z1AR comes from a spray booth where 5% of the working time is employed for the spraying of the metallic bond coat, whereas the rest of the working time of the plant is dedicated to the spraying of the ceramic top coat. On the contrary, Z2AR comes from a spray booth where 20% of the working time is employed for the spraying of the metallic bond coat, and the rest of the time is employed for the ceramic top coat. These two booths have their own downstream filtering system that collects all the oversprayed powder generated during the deposition process. The powders Z1AR and Z2AR are thus collected from these filtering systems.

In the first part of the work, Z1AR and Z2AR were investigated by using X-Ray Fluorescence (XRF, ADVANT'XP+, Thermo ARL), X-ray diffraction (XRD, PW3710, Philips), scanning electron microscopy (SEM, FEI XL-30). The analysis of the particle size distribution of the as received powders was performed by using the laser diffraction method (Mastersizer 2000 particle size analyzer with Hydro-S wet dispersion unit, Malvern Instrument Ltd., Malvern UK). The analysis of the color of the powders was performed by measuring the colorimetric CIEL*a*b* parameters (XP62, X-Rite), using D65 illuminant and CIE 1931 2° observer, following the CIE recommendations and the ASTM E308-85 [19,20]. L* describes the brightness of the color (L* = 0 for black; L* = 100 for white), a* describes the red (a* = 120) - green (a* = -120) component and b* describes the yellow (b* = 120) -blue (b* = -120) component of the color. The colors have been compared through the calculation of ΔE parameter [19].

Subsequently, physical treatments of sieving were performed in order to separate pure zirconia from pollutant particles. The sieving was performed through a set of vibrational laboratory machine (Retsch, AS200), using three different sieves in column (38, 45 and 75 μm), for a vibration time of 8 hours.

After the sieving, all the fraction of both the as received powders has been characterized following the same procedure done for the as received powders.

After characterization of all the fractions, the purest powders have been collected by FRITTA ITALIA S.r.l (Fiorano Modenese, Italy) in order to prepare frits and glazes, starting from a standard formulation for white frits and glazes. Table 1 shows the standard frit chemical compositions taken in account in this work.

Replacements of 100% of the pure zircon were performed in the white frit employing the purest recycled powders fraction and industrial quartz as source of SiO_2. The frits obtained were named

Z1-F and Z2-F respectively coming from the purest fractions of Z1AR and Z2AR. The frits preparation was performed mixing the raw material reported in the table 1 and melting the batch at 1500°C in an industrial kiln. The liquid melts were quenched in water to obtain frits. In order to identify the characteristic points of sintering, softening, sphere, half-sphere and melting, a hot-stage microscopy analysis was performed on the frits (Expert System Solutions, Misura HSM) at the heating rate of 10°C/min until 1200°C [21]. In order to verify the color of the frits they were applied onto a green porcelainzed stoneware body through an airbrush following the procedure already reported in the previous study [18]. The color of the frits, after application on the ceramic substrate was measured with the same method used for the powders.

The frits were mixed with others industrial raw material as shown in Table 2, and water in an industrial mill, in order to obtain the glazes: STD-GG indicate the standard glossy glaze, whereas STD-OG indicate the standard opaque glaze. Considering the formulations as shown in Table 2 the frit taken in account for the substitution of the raw material with the waste powders is named as "Frit", and also the zircon as raw material has been substituted with a stoichiometric combination of silica and waste zirconia.

The slurries were deposited on a dry green ceramic support by airless method by Ceramica Fondovalle (Torre Maina, Italy). The ceramic tiles were fired in an industrial kiln for 54 minutes, reaching the maximum temperature of 1215°C. The characterization of the glazes was performed using a multiple techniques approach. The crystalline phases formed in the samples were identified by X-ray diffraction (XRD, PW3710, Philips) and scanning electron microscope (SEM, FEI XL-30). The analysis of the color of the glazes was performed by measuring the colorimetric CIEL*a*b* parameters (XP62, X-Rite), using D65 illuminant and CIE 1931 2° observer, following the ASTM E 308-85 [19,20]. Spectral reflectance of each sample was measured using a UV-Vis-NIR spectrophotometer (Jasco V 670) with a 150 mm integrating sphere, in

accomplishment to ASTM E903 (ASTM International PA, 2004). The solar reflectance value ρ_{sol} of every surface was calculated by integrating over the range from 300 to 2500 nm the measured spectral reflectivity ρ_λ (defined as the ratio of reflected part and total amount of incident radiation at the considered wavelength λ), weighted by the standard spectral irradiance of the sun at the earth surface, $I_{sol,\lambda} [Wm^{-2} nm^{-1}]$ described by the AM1GH irradiance spectrum [22].

3.Results and discussion

3.1 As received zirconia powders characterization

The particle size analysis of the as-received overspray zirconia revealed a monomodal grain size distribution as shown in Figure 1 and Figure 2 for Z1AR and Z2AR respectively. The grain size parameters D10, D50 and D90 are shown in Table 3 for both the samples. Considering the results as presented in Table 3 and Figure 1 and Figure 2 , the particle size distribution of zirconia waste powders are coarser than pure zirconium silicate used in the ceramics industry, which usually presents a D50 value of around 10 microns. Moreover the sample Z2AR show a widespread grain size distribution, in respect of Z1AR.

The chemical analyses of the samples are shown in Table 3. Powder Z2AR contains higher amount of chromophore oxides than Z1AR, since it shows Ni, Co and Cr oxides. The presence of these oxides in Z2AR is probably due to the fact that from that spray booth a more polluted powder is collected, since more working time is dedicated to the spraying of the metallic bond coat. In Table 3 also the colorimetric parameters are shown. These parameters confirms in part the results of the chemical analysis, because Z2AR that is the sample with the highest amount of chromophore ions it is also the darker one, because the L* value is lower that the L* value of Z1AR sample. The XRD patterns of both the samples are the same, as can be seen in Figure 3

and Figure 4 respectively, so no difference in the level of pollutant can be detected with X-Ray diffraction. The general results for both the samples are that the powders are composed mainly by tetragonal Zirconia. This crystalline phase shows also two double peaks, as highlighted in the circles in Figure 3 and Figure 4, that are associated with crystalline phases that underwent to a thermal spray process, as previously reported [18].

Figure 5 and Figure 6 show the SEM images of Z1AR and Z2AR respectively at two different magnification 800X and 2000X. The SEM observation of as received zirconia reveals the presence of spherical, agglomerated and irregular shaped grains; moreover broken grains and pieces of sintered powders are present as well. From the characterization collected at this point Z2AR sample shows a higher presence of some contamination particles, due to the different coloration and morphology, with respect of pure zirconia powders.

3.2 Sieved zirconia powders characterization

Table 4 shows the parameters analyzed for the sieved fraction of Z1AR. For first the grain size parameters of all the sieved fraction confirms the effectiveness of the sieving, because, for each fraction of powder, D90 is more or less equal to the dimension of the following sieve. Moreover is important to underline that the fraction with the higher amount of sieved powder is the one <38 μm. This fraction is also the less polluted from metallic oxides, considering the higher amount of ZrO_2 in the XRF results, and the brighter one in color, considering its highest value of L*.The powders <38 μm and >38 μm show similar data, in this case the sieving process does not strongly increase the purity of the powders, in fact we have to consider the instrumental error of the XRF

technique that is 0.3 wt%. In particular observing the optical microscopy images, the amount of contamination particle decrease in the powder sieved through 45μm sieve. This means that the black particles have more or less dimension higher than 45 μm, so it is possible to "clean" the as-receive powders. This result is also confirmed by the chemical analysis of the sieved powders. In fact it is possible to observe that lower is the particle size, higher is the purity of the waste zirconia. decreasing the particle size distribution the purity of the waste zirconia increase. Moreover the color is depending on the grain size distribution, also visible in the optical image, and confirmed by CIELab parameters. Considering all this results, for Z1AR we can assess that the fractions < 38 μm and >38 μm are the cleanest and can be used to formulate frits suitable for white glaze. These fractions together collect the 69.16% of Z1AR as shown in Table 4.

Table 5 shows the parameters analyzed for the sieved fraction of Z2AR. Also in this case the grain size parameters of all the sieved fraction confirms the effectiveness of the sieving, because, for each fraction of powder, D90 is more or less equal to the dimension of the following sieve. In spite of Z1AR, the fractions of Z2AR with the higher amount of sieved powder are >38 μm and >45μm. Also in this case the sieved fraction < 38μm is the less polluted from metallic oxides, considering the higher amount of ZrO_2 but also the lower content of the chromophore cobalt oxide in the XRF results. Also for Z2AR sieved fraction it is possible to observe that decreasing the particle size distribution the purity of the waste zirconia increases. Moreover, also the colour is depending on the grain size distribution, as well visible in the optical image, and confirmed by CIELab parameters. As for Z1AR powder the amount of contamination particle decrease in the powder sieved through 45μm, for Z2AR the amount of pollutant decrease significantly in the powder sieved <38 μm. Considering all this results, for Z2AR we can assess that the fraction < 38 μm is the cleanest and can be employed to formulate frits suitable for white glaze. This

fraction collects the 13.21% of Z2AR as shown in Table 5. As a result, considering the amount of

the cleanest powder sieved for Z1AR and for Z2AR we expect to recover less clean powder from

Z2AR than Z1AR.

3.3 Frits and glazed tiles characterization

In Table 6 the hot stage microscope characterization of the two studied frits has been shown, in

comparison with the data of the standard frits. It can be observed that the thermal behavior (see

characteristic temperatures) of the new frits containing the purest fraction of waste zirconia

instead of pure raw material is quite similar to the behavior shown by the standard industrial frits,

independently from the type of waste zirconia employed (Z1-F or Z2-F). For this reason we can

assume that the thermal behavior of the glazes during firing will be similar and no further

changes will be necessary to employ these frits in industrial application. The reasons for this

claim are principally two: the first reason is that we must consider that the materials taken in

consideration in this study are industrial materials, that work at quite high temperature in

industrial kiln, where a variation range of +/-50°C must be considered as acceptable. The second

reason is that when glazes for ceramic tile are studied generally sphere, half-sphere and melting

are the most important temperature to be evaluated and compared. For this reason, higher

discrepancy for sintering and softening can be evaluated as secondary.

In table 7 the results obtained through the color measurement of the frits have been shown after

the application on ceramic support. From this results we can observe that a relevant decrease can

be seen for L* coordinate and a significantly increase can be estimated for b* coordinate. A

strong difference in terms of color can be observed when Z2-F is compared with the white

standard frit.

In Figure 7 a comparison of the glossy glazes obtained with STD-F, Z1-F and Z2-F respectively,

following the composition shown in Table 2, is shown. From Figure 7 it is possible to see that Z1-GG is white and no coloration is shown if compared with the standard white glaze. On the contrary Z2-GG has shown a strong greenish coloration. Similar results can be achieved using the same frits to produce opaque glazes as shown in Figure 8. The change in coloration can be measured and is confirmed through the color parameters as shown in Table 8.

Considering Table 8 and the values obtained from Z2-GG and Z2-OG a strong decrease can be seen for L* coordinate and a relevant increase can be estimated for b* coordinate, both for glossy and opaque glaze. These differences indicate respectively a decrease in brightness and an increase in the greenish tone. About color Also the ΔE value can be observed, in order to consider an objective measurement of the difference in color between a glaze and its reference. Higher is the ΔE value and higher is the difference between the two colors compared. ΔE value in the case of Z1-GG is 1.54 that is below the limit of acceptance for the human eye (ΔE =3) [23], for this reason the two colors can be estimated as the same. On the contrary the ΔE value associated with Z2-GG is 18.11, so strongly over the limit of acceptance for the human eye. The same evaluations can be done for Z1-OG and Z2-OG respectively. The change in coloration can be explained considering the presence of chromophore elements in the sieved powders employed in Z2-F frit, as cobalt and chromium in particular, even if present in low amount as shown in Table 5 [24-25]. Taking in account the light greenish coloration achieved we can assume also that in this case cobalt ion is 4-fold coordinated [26]. Considering this result, the frit formulated with the sieved fraction of Z2AR powder must be discarded because, even if low, the amount of metallic pollutant prevents the achievement of a white glaze. Because of this result the further characterizations have been done only on the white glazes obtained Z1-GG and Z1-OG. The reflectance spectra of the white glazes obtained are shown in Figure 9 and Figure 10 considering respectively glossy and opaque glaze.

From Figure 9 and Figure 10 it is possible to see that the reflectance spectra of the glazes are overlapped in both cases in the visible region (400-700nm), no relevant changes can be seen for this property when pure zircon is substitute with the sieved fraction of Z1AR and quartz.

In order to evaluate any change in microstructure XRD and SEM measurement has been performed on all the white glaze samples obtained. In Figure 11 the XRD pattern of the samples STD-GG and Z1-GG have been shown.

About the glossy samples shown in Figure 11 it is possible to see that both the pattern are characterized by a strong glassy band and the only one mineralogical phase identified is Zircon (ICDD: 01-083-1374), in fact all the peaks present in the patterns shown in Figure 11 can be associated with that mineralogical phase. In Figure 12 the XRD pattern of the samples STD-OG and Z1-OG have been shown.

About the opaque samples, as shown in Figure 12 it is possible to achieve that the mineralogical phases are two: Zircon (ICDD: 01-083-1374) and Anorthite (ICDD:00-018-1202). The difference in terms of mineralogical phases between glossy and opaque glaze is due to different raw material inside the glaze employed to obtain the desired surface appearance. Also an important difference in terms of glassy phases is present, in fact as expected the glassy phases in higher for the glossy glazes in respect of the opaque ones. This result can be evaluated observing the band around 25-27 °2θ, that is typically associated with the presence of silicate glassy phase. As expected from other studies [27] X-ray diffraction studies that have examined glazes containing both zircon and zirconia have demonstrated that zircon is the final opacifier crystal, regardless of which zirconium species is present in the glaze formulation. Other researches have shown that the amount of zircon or zirconium oxide that forms initially is dependent on the $SiO_2:ZrO_2$ ratio in

the frit. Glazes with lower silica contents have a tendency, initially, to produce zirconium oxide phases, whereas higher silica glazes initially produce zircon crystals during heating. In both cases, however, zircon was, again, the major opacifier phase in the final glaze. In Figure 13 and Figure 14 respectively the SEM images of the glossy and opaque glazes respectively has been shown.

The SEM images considered are in backscattered electron in order to identify the presence of crystals inside the microstructure of the glazes. The SEM images obtained from the samples Z1-GG and Z1-OG are completely similar to respectively STD-GG and STD-OG. This result demonstrates that the substitution of pure zirconium silicate with a sieved fraction of YSZ and quartz does not change the glaze microstructure. As expected, important difference can be considered if we compare the microstructure of the glossy glaze with the microstructure of the opaque glaze. As previously seen in the XRD analysis the opaque glaze is characterized by a strong presence of crystals than the glossy glaze. In particular in Figure 14 that refers to the opaque glazes analyzed needle-shape crystals and rod-shape crystal can be clearly seen in both the samples. For similar system, in literature the needle-shape crystals are associated with the presence of zircon crystals [28-30], whereas the rod-shape crystals can be associated with Anorthite [6]. On the contrary, in the glossy glazes only zircon crystals can be seen on the surface, as shown in Figure 13. In fact as shown from the EDS analysis in Figure 15, the crystals show the chemical composition of zircon, whereas the glassy phase shows the chemical composition of the glaze. The larger zircon crystal present in the glossy glazes can derive from an aggregation of zircon that is added in the glaze formulation as raw material as shown in Table 2. In fact the typical grain size of this industrial powder is about 1,25 μm (D50).

Conclusion

In this study the feasibility of valorizing and recycling YSZ thermal spray waste, in relevant amount, to high value products as white glazes for ceramic tile has been demonstrated. As shown in previously studies [18] YZS thermal spray waste cannot be employed in a 100% substitution in frits or glaze for white glaze formulation due to the high amount of metallic pollutant. In this study we have demonstrated that the mechanical action of sieving is effective in order to remove the metallic pollutant from at least 59.16% of the Z1AR thermal spray waste. The purified powder can be employed in a 100% substitution of zirconia, in combination with quartz. In fact, colour measurement, SEM and XRD analysis in particular have shown that the parameters are in the same range of the standard industrial white glazes, both for glossy and opaque types. As confirmed by previous study [26] zircon is the main crystalline phase inside the glaze microstructure, regardless of which zirconium species is present in the glaze formulation.

The analysis of Z2AR, demonstrate that if the pollutant is in too high amount the powder cannot be recycled for white frits and glazes, so other studies will be necessary to find other field of application for this waste powder.

Taking in account only the waste powder from Turbocoating, about 480 Kg is the amount of waste powder that can be recycled for white frits in a month through mechanical sieving. Following the formulations employed in this study this means that the waste powders recycled in one month can cover the production of approximately 480.000 mq of ceramic tiles. As only the Italian production of ceramic tile during 2015 reached 397 millions/mq [31], the recycled powder can cover approximately the 1,33% of only the Italian production of ceramic tile.

As future prospective technological characterizations of the glazes will be done in order to complete the comparison between standard product and product obtained with waste powders.

Acknowledgments

References

1. Rawlings RD, Wu JP, Boccaccini AR. Glass-ceramics: Their production from wastes—A Review. *J. Mater. Sci.* 2006;41:733–761.

2. Romero M, Rincon JM, Acosta A. Crystallization of a zirconium based glaze for ceramic tile coating. *J. Eur. Ceram. Soc.* 2003;23:1629–1635.

3. Parmalee CW. Ceramic Glazes. 3thed. Boston, NY: Cahners Books; 1973.

4. Shaw K. Ceramic Glazes. Amsterdam, NL: Elsevier Science; 1971.

5. Garcia Sainz J. Physical-chemical characteristics of ceramic glazes and their influence on quality of floor and wall tiles. *Tile Brick Int.* 1990; 6:21-22.

6. Selli NT. Development of anorthite based white porcelain stoneware tile compositions. *Ceram. Int.* 2015;41:7790–7795.

7. Castilone RJ, Sriram D, Carty WM, Snyder RL. Crystallization of zircon in stoneware. *J. Am. Ceram. Soc.* 1999;82:2819–2824.

8. Jacobs CW. Opacifying Crystalline Phases Present in Zirconium-Type Glazes. *J. Am. Ceram. Soc.* 1954;37:216–220.

9. El-Defrawi SA, Abd El-Fattah WI. Pinholes and introduction of albite in double firing zircon-glazed tiles. *Silicates Industriels*. 1993;58:31-36.

10.El-Defrawi SA, Serry MA, Abd El-Fattah WI, Weisweiler W. Microchemistry and microstructure of some opaque glaze/tile interfaces in relation to their physical properties. *Ceram. Int.* 1995;21:69–75.

11. T.Z. Minerals International Pty Ltd, Zircon supply/demand report. 2016.

12. Shackelford JF, Doremus RH. Ceramic Glass Materials. New York, NY: Springer; 2008.

13. Padture NP, Gell M, Jordan EH. Thermal Barrier Coatings for Gas-Turbine Engine Applications. *Science. 2002;*296:280–284.

14. Clarke DR, Levi GG. Materials Design for the Next Generation Thermal Barrier Coatings. *Annu. Rev. Mater. Res*. 2013;33:383–417.

15. Vassen R, Jarligo MO, Steinke T, Mack DM, Stoever D. Overview on advanced thermal barriercoatings. *Surf. Coat. Technol*. 2010;205:938–942.

16. Kumar V, Kandasubramanian B. Processing and design methodologies for advanced and novel thermal barrier coatings for engineering applications. *Particuology. 2016;*27:1–28.

17. Dawson T. A clean spray. *Industrial Paint & Powder*. 2006;6:10-14.

18. Siligardi C, Lusvarghi L, Giolli C, Scrivani A, Venturelli D. Recycling in ceramic glazes of zirconia overspray from thermal barrier coatings manufacturing. *J. Eur. Ceram. Soc.* 2014;34: 147–154.

19. Hunt RWG, Pointer MR. Measuring Colour. Oxford, UK: John Wiley and Sons; 2011.

20. ASTM E308-85. Standard Practice for Computing the Colors of Objects by Using the CIE System. West Conshohocken, PA: ASTM International; 1987.

21. Paganelli M. Understanding the behavior of glazes: new test possibilities using the automatic hot stage microscope MISURA. *Ind. Ceram.* 1997;17:69-73.

22. Levinson R, Akbari H, Berdahl P, Measuring solar reflectance Part I: defining a metric that accurately predicts solar heat gain, *Solar Energy*, 2010;84:1717-1744.

23. ACIMAC. Colour, pigments and colouring in ceramics. Modena, IT: SALA; 2003.

24. Huang M, Wang Z, Liu S. Reutilization of the Cr ions adsorbed on activated carbon as colorants in glass preparation. *J. Environ. Chem. Eng.* 2016;4:1555-1560.

25. Hunault M, Bauchau F, Loisel C, Herold M, Galoisy L, Newville M, Calas G. Spectroscopic Investigation of the Coloration and Fabrication Conditions of Medieval Blue Glasses. *J. Am. Ceram. Soc.* 2016;99:89–97

26. Paul A, Douglas RW. Optical absorption of divalent cobalt in binary alkali borate glasses and its relation to basicity of glass. *Phys. Chem. Glasses-Eur. J. Glass Sci. Technol. Part B. 1968;*9:21–26.

27. Sehlke KH, Tauber A.A High-Temperature X-ray Diffraction Study of Zircon-Containing Glaze Frits. *Trans. Br. Ceram. Soc*. 1969;68:53–56.

28. Sheikhattar M, Attar H, Sharafi S, Carty WM.Influence of surface crystallinity on the surface roughness of different ceramic glazes. *Mater. Charact*. 2016;118:570–574.

29. Wang S, Peng C, Xiao H, Wu J. Microstructural evolution and crystallization mechanism of zircon from frit glaze. *J. Eur. Ceram. Soc.* 2015;35:2671–2678.

30. Wang X, Chen M, Zhu S, Wang F. Phase evolution of SiO_2–Al_2O_3–ZnO–CaO–ZrO_2–TiO_2-based glass with added Y-PSZ particles. *J. Am. Ceram. Soc. 2013;*96:1456–1463.

31. ACIMAC. World production and consumption of ceramic tile. Modena, IT: SALA;2016.

LIST OF FIGURE CAPTIONS

Figure 1. Grain size distribution of sample Z1AR

Figure 2. Grain size distribution of sample Z2AR

Figure 3. XRD Pattern of sample Z1AR: t-Zr, tetragonal zirconia

Figure 4. XRD Pattern of sample Z2AR: t-Zr, tetragonal zirconia

Figure 5. SEM Images at different magnitude of sample Z1AR

Figure 6. SEM Images at different magnitude of sample Z2AR

Figure 7. Comparison of the glossy glazes obtained a) STD-GG b) Z1-GG c) Z2-GG

Figure 8. Comparison of the opaque glazes obtained a) STD-OG b) Z1-OG c) Z2-OG

Figure 9. Reflectance spectra of the white glossy glazes

Figure 10. Reflectance spectra of the white opaque glazes

Figure 11. XRD Pattern of the white glossy glazes: Zr-Si, Zirconium Silicate

Figure 12. XRD Pattern of the white opaque glazes: Zr-Si, Zirconium Silicate; A, Anorthite

Figure 13. SEM Images of sample a) STD-GG b)Z1-GG

Figure 14. SEM Images of sample a) STD-OG b)Z1-OG

Figure 15 – EDS spectra of Figure 13: (a) crystals (black circles of Figure 13) (b) glassy phase

1
2
3
4
5
6
7
8
9
10
11
12
13
14
15
16
17
18
19
20
21
22
23
24
25
26
27
28
29
30
31
32
33
34
35
36
37
38
39
40
41
42
43
44
45
46
47
48
49
50
51
52
53
54
55
56
57
58
59
60

Table 1 – Formulation of white standard frit (STD-F) (wt%)

Raw materials	STD – F (wt%)
Borax pentahydrate	16.8
Zircon	7.2
Dolomite	6.2
K-feldspar	32.5
Feldspatic flour	37.3

Table 2 – Formulation of white standard glazes: STD-GG and STD-OG (wt%)

Raw materials	STD – GG (wt%)	STD – OG(wt%)
Frit	9	10
Frit 2	1	0
Zircon	17	17
White Clay	22	22
Alumina	4	4
Caolin	10	10
Calcium Carbonate	11	11
Nepheline	24.5	24.5
Zinc Oxide	1.5	1.5

Table 3 – Properties of the as-received Zirconia powders Z1AR and Z2AR

Properties	Z1AR	Z2AR
Grain size parameters (μm)		
D10	20	3
D50	38	18
D90	67	54
XRF (wt%)		
ZrO_2	85,0	79,7
Y_2O_3	9,3	8,6
HfO_2	3,4	3,1
NiO	-	2,5
Cr_2O_3	-	2,1
Al_2O_3	0,7	1,3
Co_3O_4	-	0,8
SiO_2	0,5	1,1
Na_2O	0,3	0,4
Others	0,8	0,4
Colorimetric Parameters		
L*	91,85 ± 1,34	84,03 ± 0,98
a*	-0,94 ± 0,22	-1,09 ± 0,12
b*	18,46 ± 0,02	13,92 ± 0,42

Table 4 – Properties of the sieved fraction of Z1AR

Properties	<38μm	>38μm	>45μm	>75 μm
Sieved fraction (% Z1AR)	59.16	10.00	28.96	11.64
Grain size parameters (μm)				
D10	10	27	36	12
D50	20	38	52	72
D90	36	54	76	132
XRF (wt%)				
ZrO_2	85.6	84.8	84.3	82.6
Y_2O_3	9.3	9.4	9.2	9.1
HfO_2	3.2	3.1	3.3	3.1
NiO	-	-	-	-
Cr_2O_3	-	-	-	-
Al_2O_3	0.4	1.2	1.8	3.7
Co_3O_4	-	-	-	-
SiO_2	0.4	0.3	0.3	0.3
Na_2O	0.3	0.3	0.3	0.3
Others	0.8	0.9	0.8	0.9
Colorimetric Parameters				
L*	89.4 ± 0.27	88.90 ± 0.42	86.40 ± 0.34	83.00 ± 0.24
a*	-0.5 ± 0.04	-1.0 ± 0.07	-0.2 ± 0.05	-0.2 ± 0.03
b*	12.5 ± 0.23	12.90 ± 0.43	12.60 ± 0.24	11.30 ± 0.29

Optical Microscope Images 35x

Table 5 – Properties of the sieved fraction of Z2AR

Properties	<38μm	>38μm	>45μm	>75 μm
Sieved fraction (% Z2AR)	13.21	48.58	40.58	13.21
Grain size parameters (μm)				
D10	11	30	43	70
D50	22	43	60	95
D90	40	61	83	128
XRF (wt%)				
ZrO_2	83.6	81.8	80.6	79.4
Y_2O_3	9.1	9.0	8.7	8.8
HfO_2	3.6	3.1	3.1	3.3
NiO	0.5	0.5	0.5	0.4
Cr_2O_3	0.3	0.3	0.3	
Al_2O_3	0.3	/	/	/
Co_3O_4	1.0	2.8	2.8	3.2
SiO_2	0.8	0.9	2.5	3.1
Na_2O	0.3	0.9	0.9	1.2
Others	0.5	0.6	0.6	0.6
Colorimetric Parameters				
L*	66.6 ± 0.07	68.80 ± 0.43	68.7 ± 0.24	68.5 ± 0.34
a*	-1.8 ± 0.10	-1.8 ± 0.05	-1.5 ± 0.08	-1.7 ± 0.02
b*	11.8 ± 0.25	12.50 ± 0.27	11.2 ± 0.45	13.60 ± 0.56

Optical Microscope Images 35x

Table 6 – Hot stage microscope characterization of the frits

	Sintering (°C)	Softening (°C)	Sphere (°C)	Half sphere (°C)	Melting (°C)
STD-F	894	935	1109	1307	1338
Z1-F	803	1001	1151	1344	1377
Z2-F	794	877	1115	1306	1349

Table 7 – Hunter parameters of the frits investigated

FRITS	L*	a*	b*	ΔE
STD –F	88.73 ± 0.14	-0.62 ± 0.02	1.55 ± 0.05	/
Z1-F	87.32 ± 0.09	-0.64 ± 0.12	1.11 ± 0.13	1.13
Z2-F	70.45 ± 0.11	-6.54 ± 0.09	7.23 ± 0.05	20.04

Table 8 – Hunter parameters of the glazes investigated

GLAZES	L*	a*	b*	ΔE
GLOSSY				
STD - GG	90.19 ± 0.53	-0.66 ± 0.03	-0.28 ± 0.06	/
Z1 - GG	90.33 ± 0.44	-0.70 ± 0.07	0.43 ± 0.12	1.54
Z2 - GG	73.18 ± 0.09	-3.19 ± 0.06	5.42 ± 0.09	18.12
OPAQUE				
STD - OG	86.32 ± 0.12	-0.65 ± 0.03	0.83 ± 0.04	/
Z1 - OG	86.41 ± 0,16	0.66 ± 0.02	0.92 ± 0.04	1.32
Z2 - OG	70.18 ± 0.23	-2.59 ± 0.12	6.38 ± 0.06	17.37
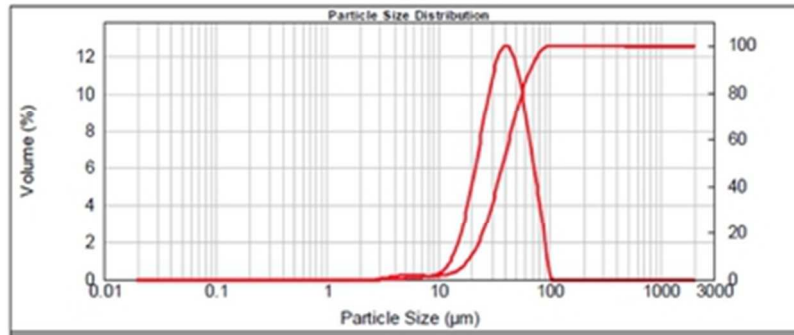
Grain size distribution of sample Z1AR
Figure 1
34x14mm (300 x 300 DPI)

1
2
3
4
5
6
7
8
9
10
11
12
13
14
15
16
17
18
19
20
21
22
23
24
25
26
27
28
29
30
31
32
33
34
35
36
37
38
39
40
41
42
43
44
45
46
47
48
49
50
51
52
53
54
55
56
57
58
59
60
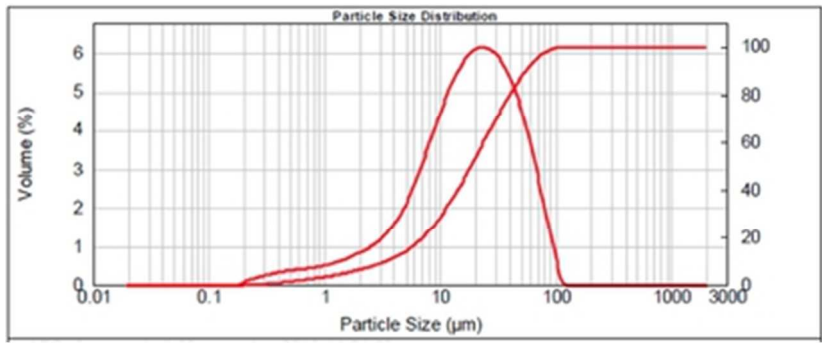
Grain size distribution of sample Z2AR
Figure 2
34x14mm (300 x 300 DPI)
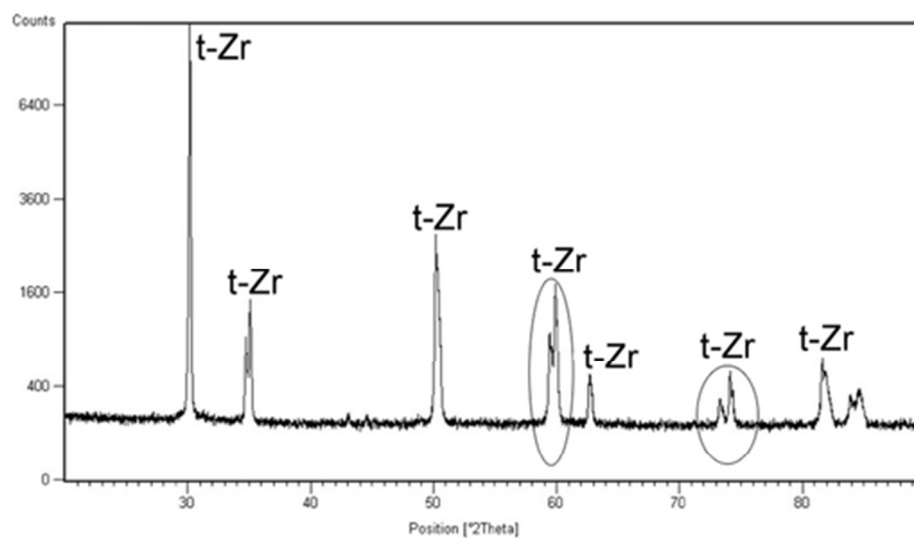
XRD Pattern of sample Z1AR: t-Zr, tetragonal zirconia
Figure 3
47x26mm (300 x 300 DPI)
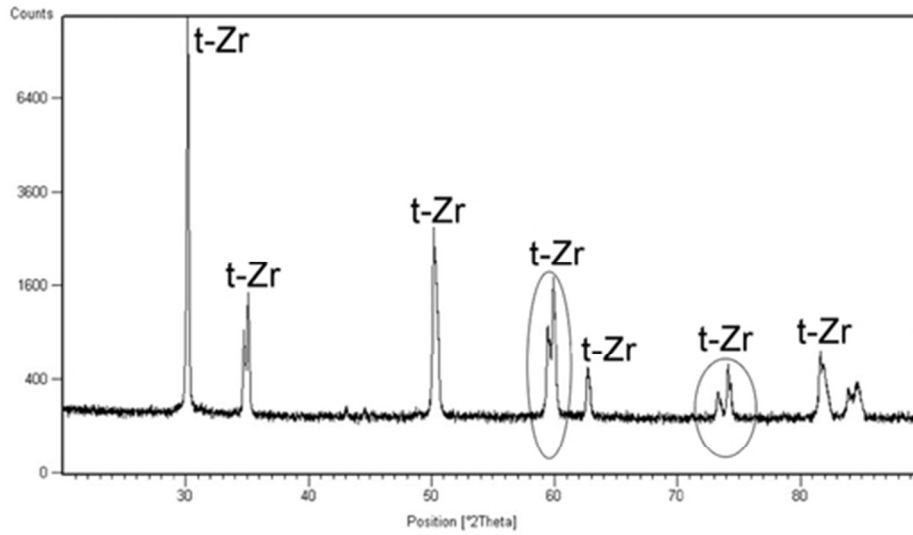
XRD Pattern of sample Z2AR: t-Zr, tetragonal zirconia
Figure 4
47x26mm (300 x 300 DPI)
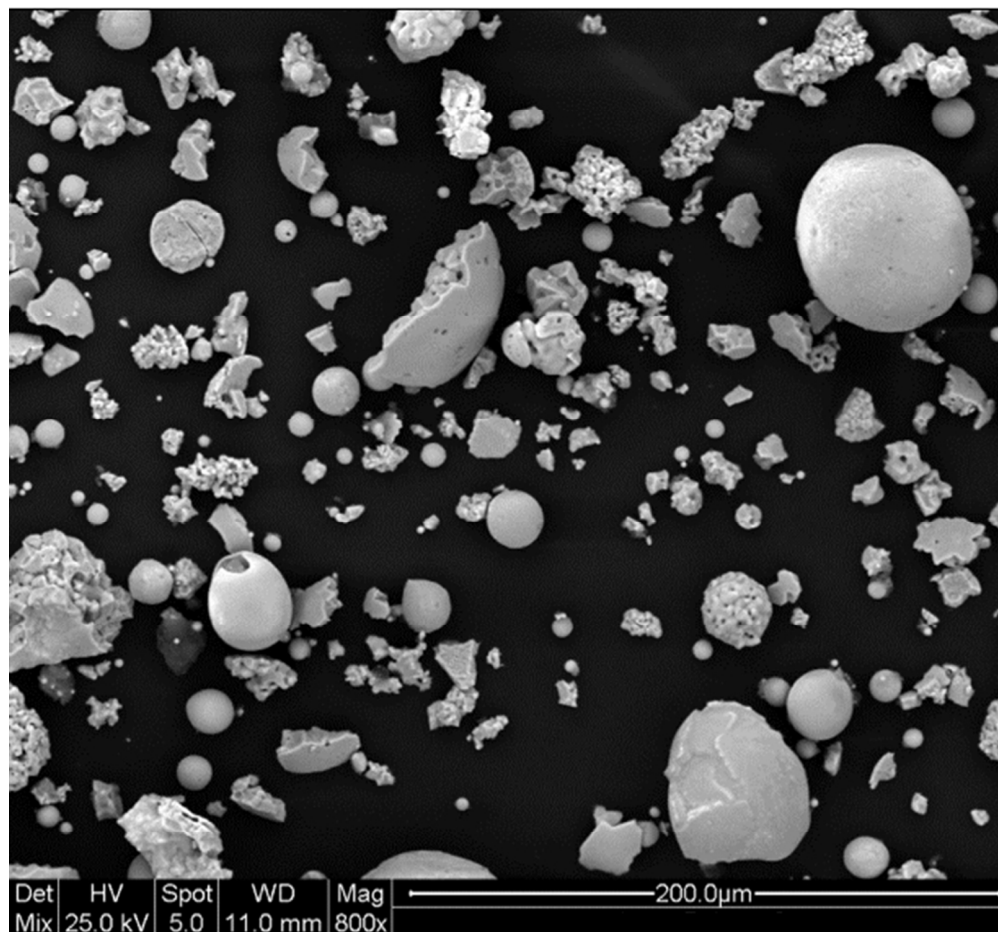
Figure 5. SEM Images at different magnitude of sample Z1AR
Figure 5
85x78mm (300 x 300 DPI)

1
2
3
4
5
6
7
8
9
10
11
12
13
14
15
16
17
18
19
20
21
22
23
24
25
26
27
28
29
30
31
32
33
34
35
36
37
38
39
40
41
42
43
44
45
46
47
48
49
50
51
52
53
54
55
56
57
58
59
60
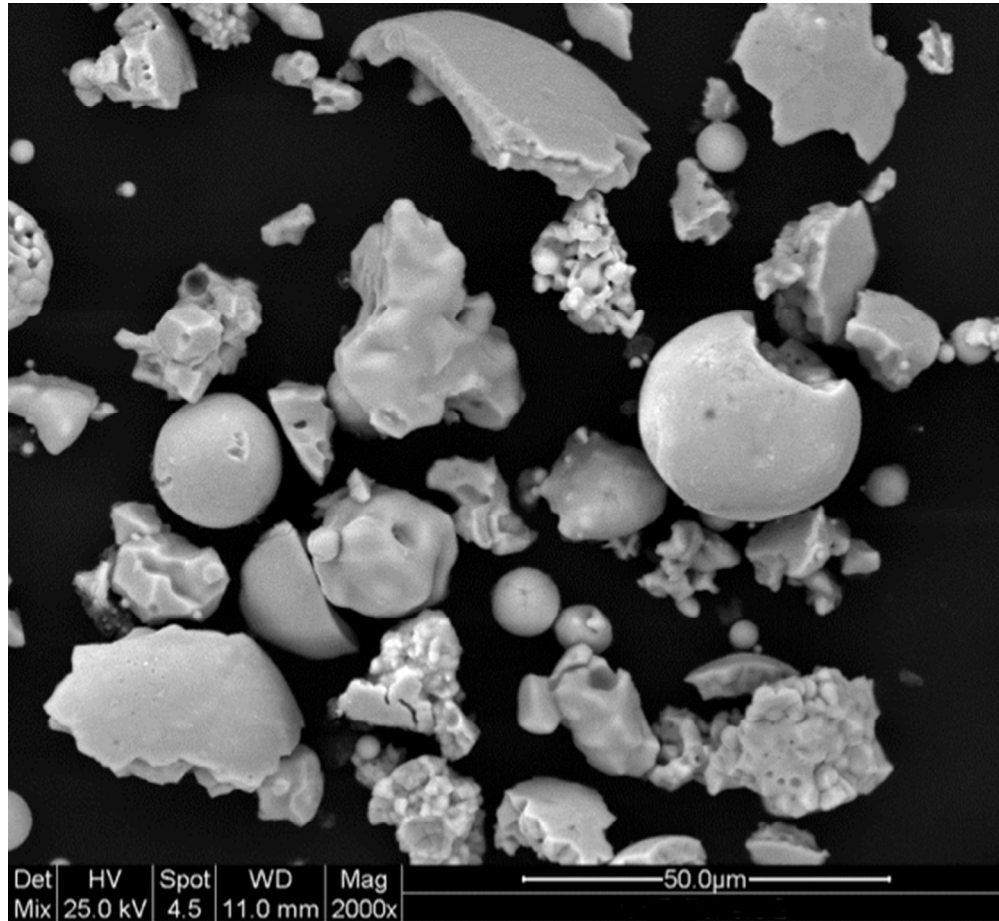
Figure 5. SEM Images at different magnitude of sample Z1AR
Figure 5
85x78mm (300 x 300 DPI)
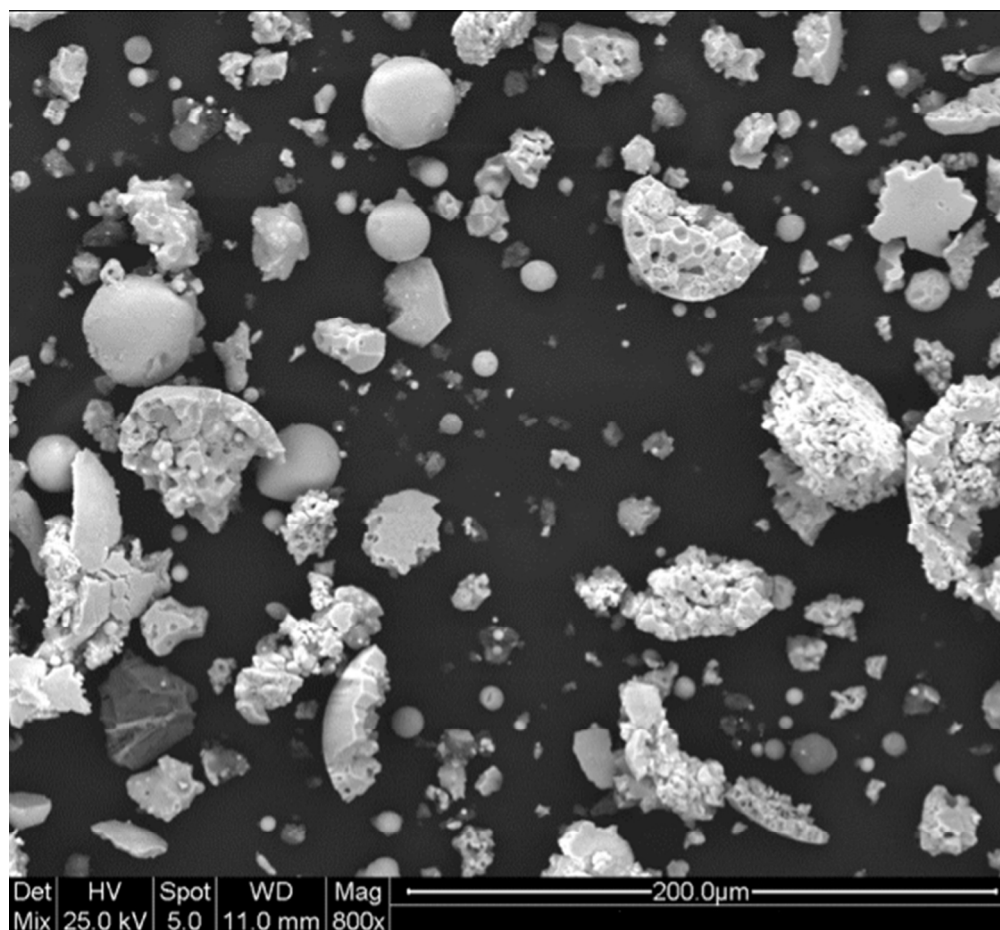
Figure 6. SEM Images at different magnitude of sample Z2AR
Figure 6
85x78mm (300 x 300 DPI)

1
2
3
4
5
6
7
8
9
10
11
12
13
14
15
16
17
18
19
20
21
22
23
24
25
26
27
28
29
30
31
32
33
34
35
36
37
38
39
40
41
42
43
44
45
46
47
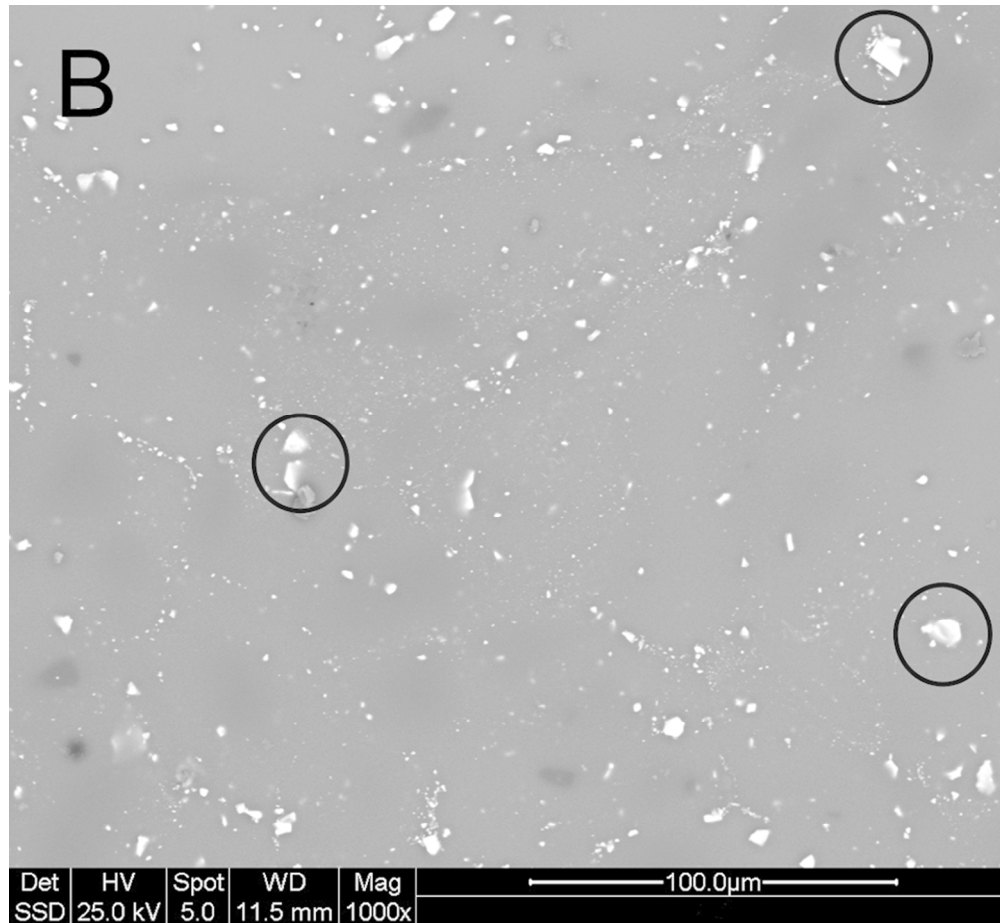48
49
50
51
52
53
54
55
56
57
58
59
60
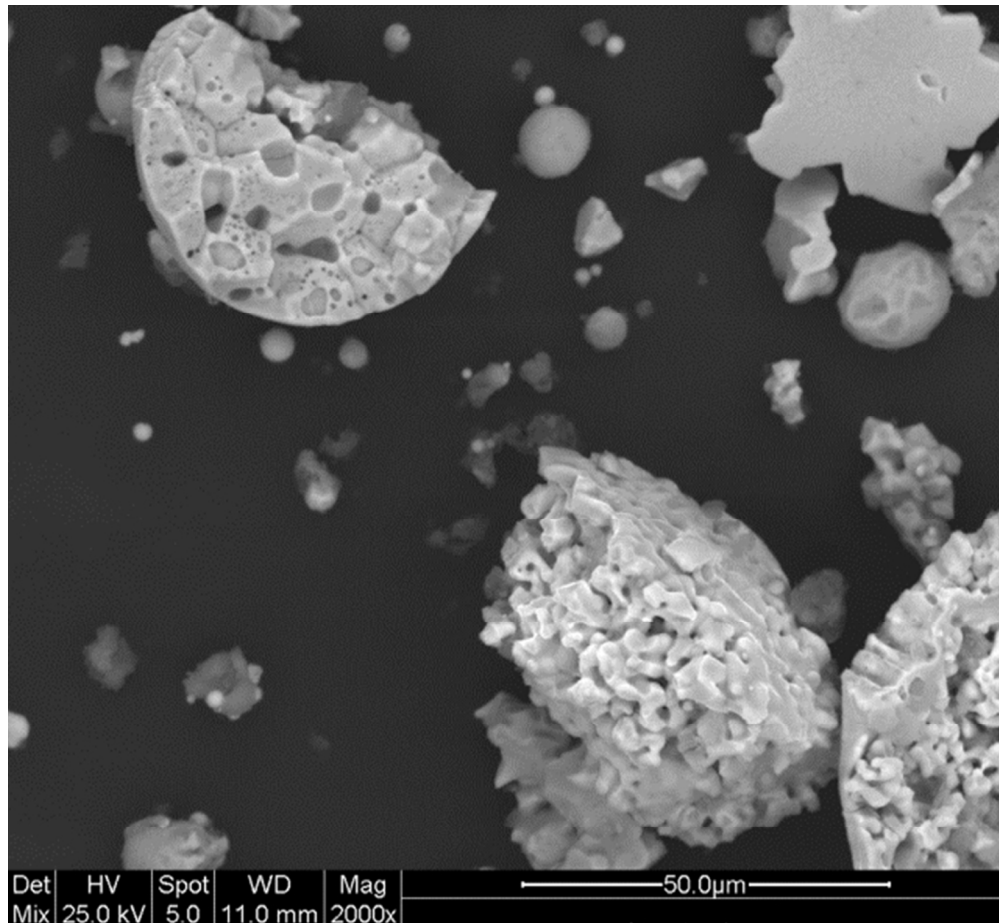
Figure 6. SEM Images at different magnitude of sample Z2AR
Figure 6
85x78mm (300 x 300 DPI)
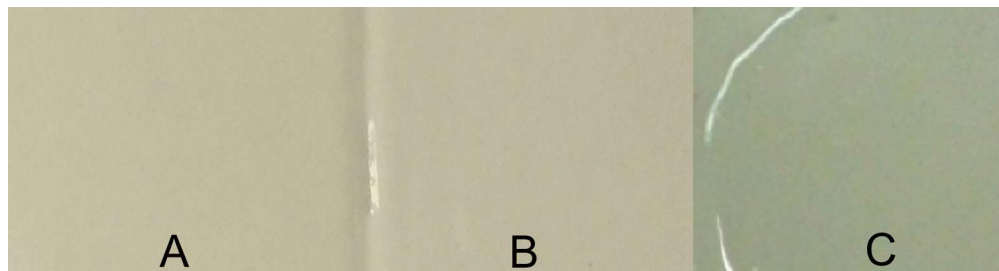
Figure 7. Comparison of the glossy glazes obtained a) STD-GG b) Z1-GG c) Z2-GG
Figure 7
177x46mm (300 x 300 DPI)
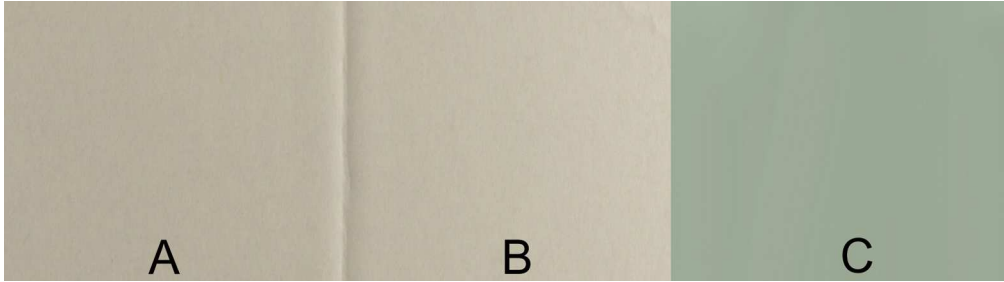
Figure 8. Comparison of the opaque glazes obtained a) STD-OG b) Z1-OG c) Z2-OG
Figure 8
177x49mm (300 x 300 DPI)
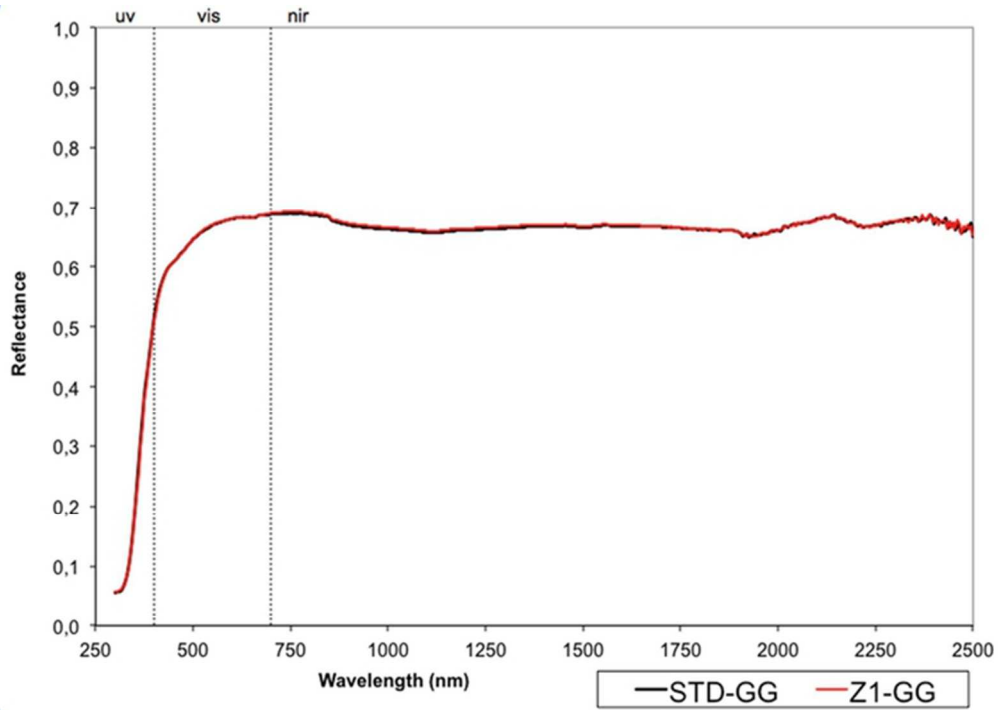
Figure 9. Reflectance spectra of the white glossy glazes
Figure 9
60x43mm (300 x 300 DPI)
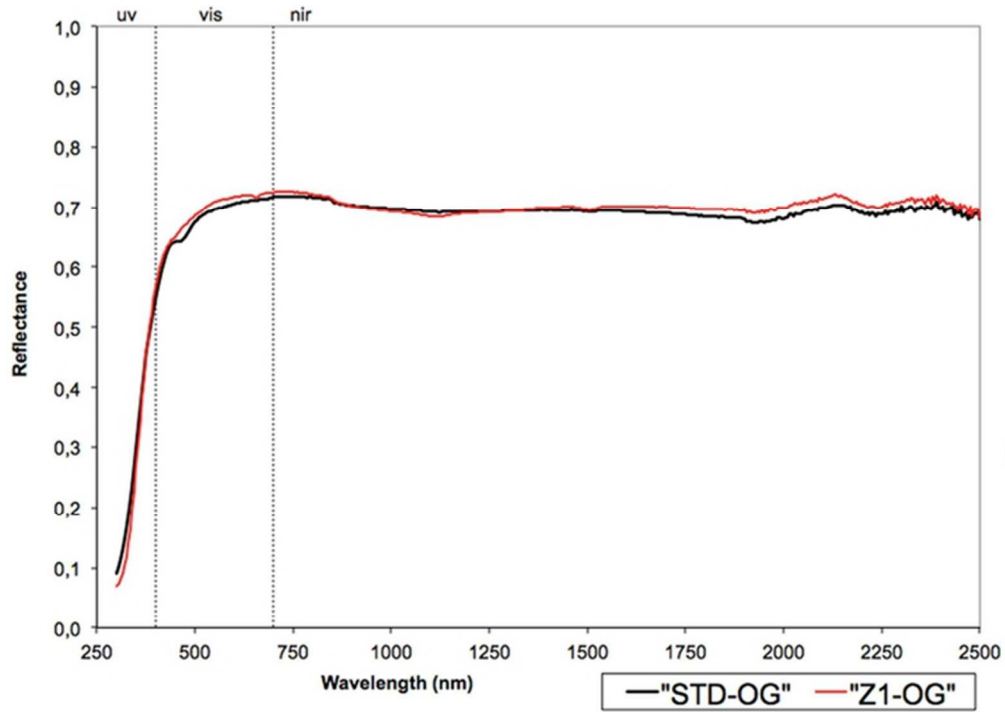
Figure 10. Reflectance spectra of the white opaque glazes
Figure 10
60x43mm (300 x 300 DPI)
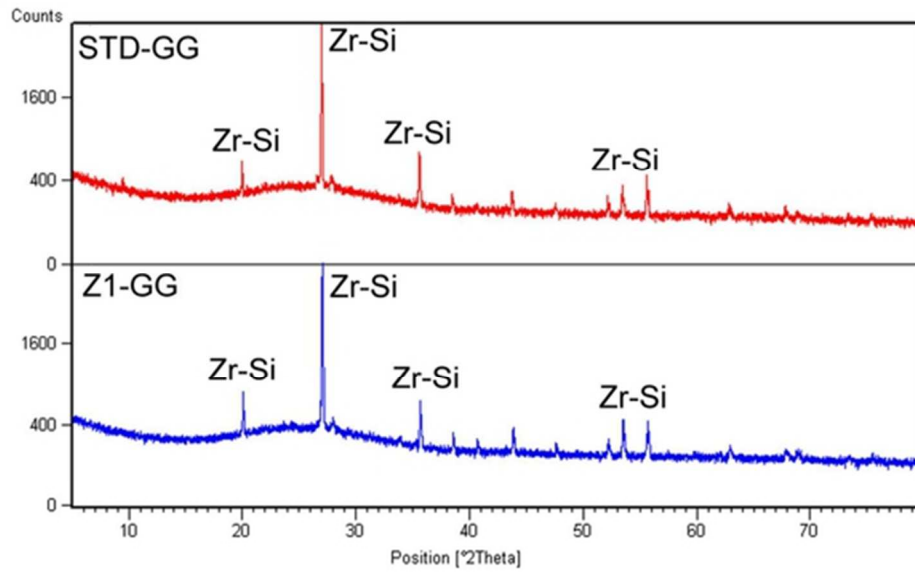
Figure 11. XRD Pattern of the white glossy glazes: Zr-Si, Zirconium Silicate
Figure 11
53x33mm (300 x 300 DPI)
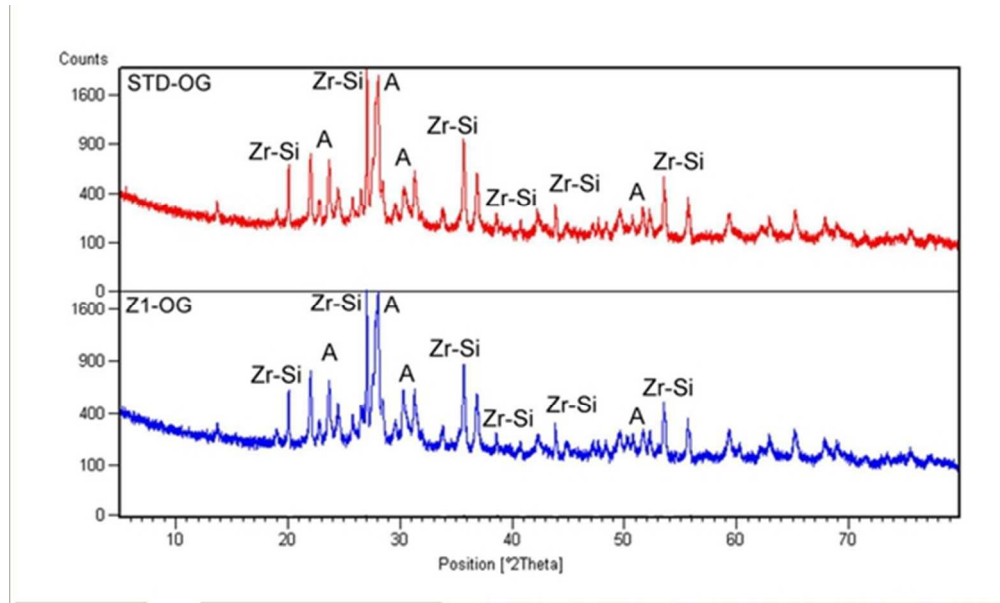
Figure 12. XRD Pattern of the white opaque glazes: Zr-Si, Zirconium Silicate; A, Anorthite
Figure 12
50x30mm (300 x 300 DPI)

Figure 13. SEM Images of sample a) STD-GG b)Z1-GG
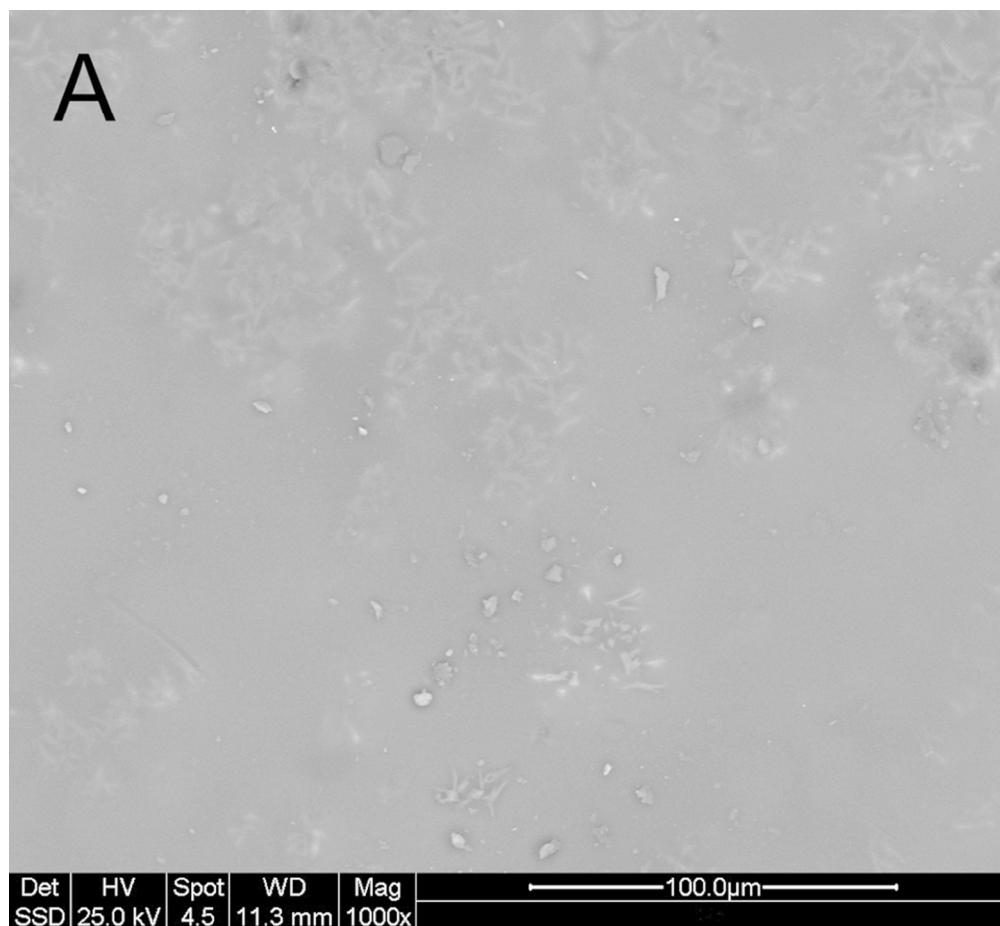Figure 13
85x78mm (300 x 300 DPI)

Figure 13. SEM Images of sample a) STD-GG b)Z1-GG
Figure 13
85x78mm (300 x 300 DPI)

1
2
3
4
5
6
7
8
9
10
11
12
13
14
15
16
17
18
19
20
21
22
23
24
25
26
27
28
29
30
31
32
33
34
35
36
37
38
39
40
41
42
43
44
45
46
47
48
49
50
51
52
53
54
55
56
57
58
59
60

Figure 14. SEM Images of sample a) STD-OG b)Z1-OG
Figure 14
85x78mm (300 x 300 DPI)

1
2
3
4
5
6
7
8
9
10
11
12
13
14
15
16
17
18
19
20
21
22
23
24
25
26
27
28
29
30
31
32
33
34
35
36
37
38
39
40
41
42
43
44
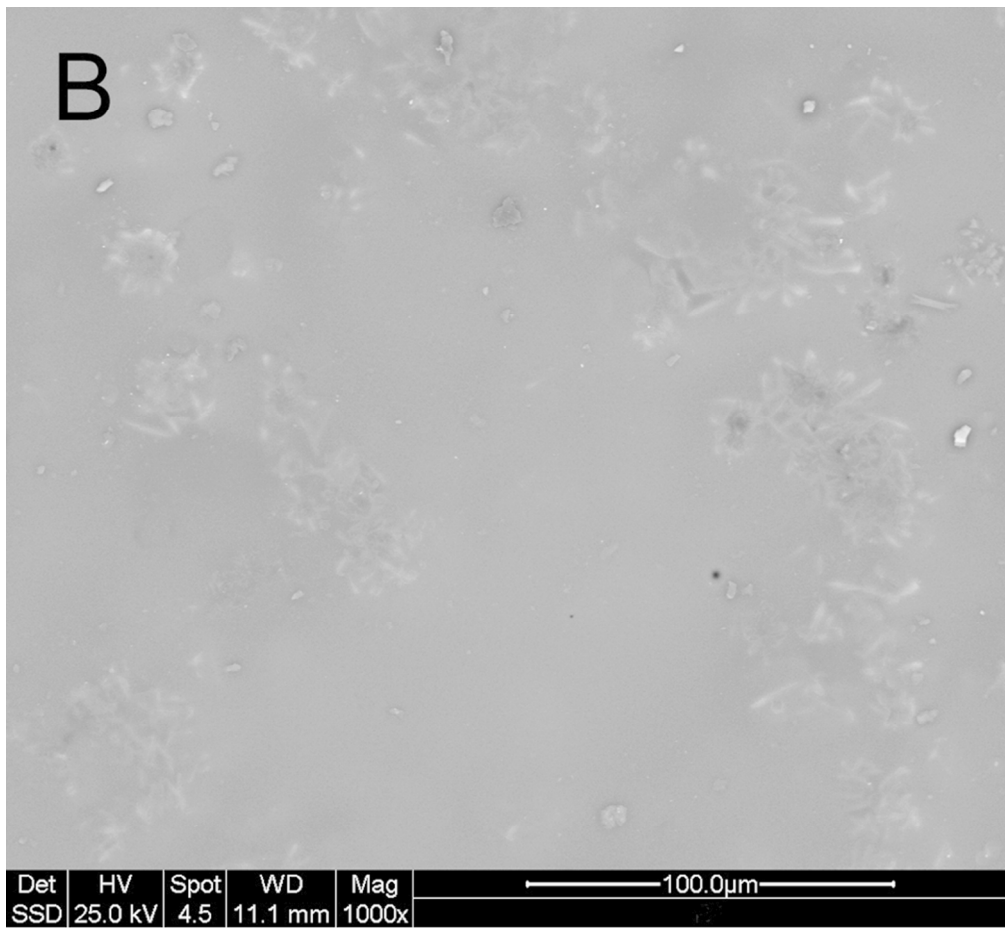45
46
47
48
49
50
51
52
53
54
55
56
57
58
59
60

Figure 14. SEM Images of sample a) STD-OG b)Z1-OG
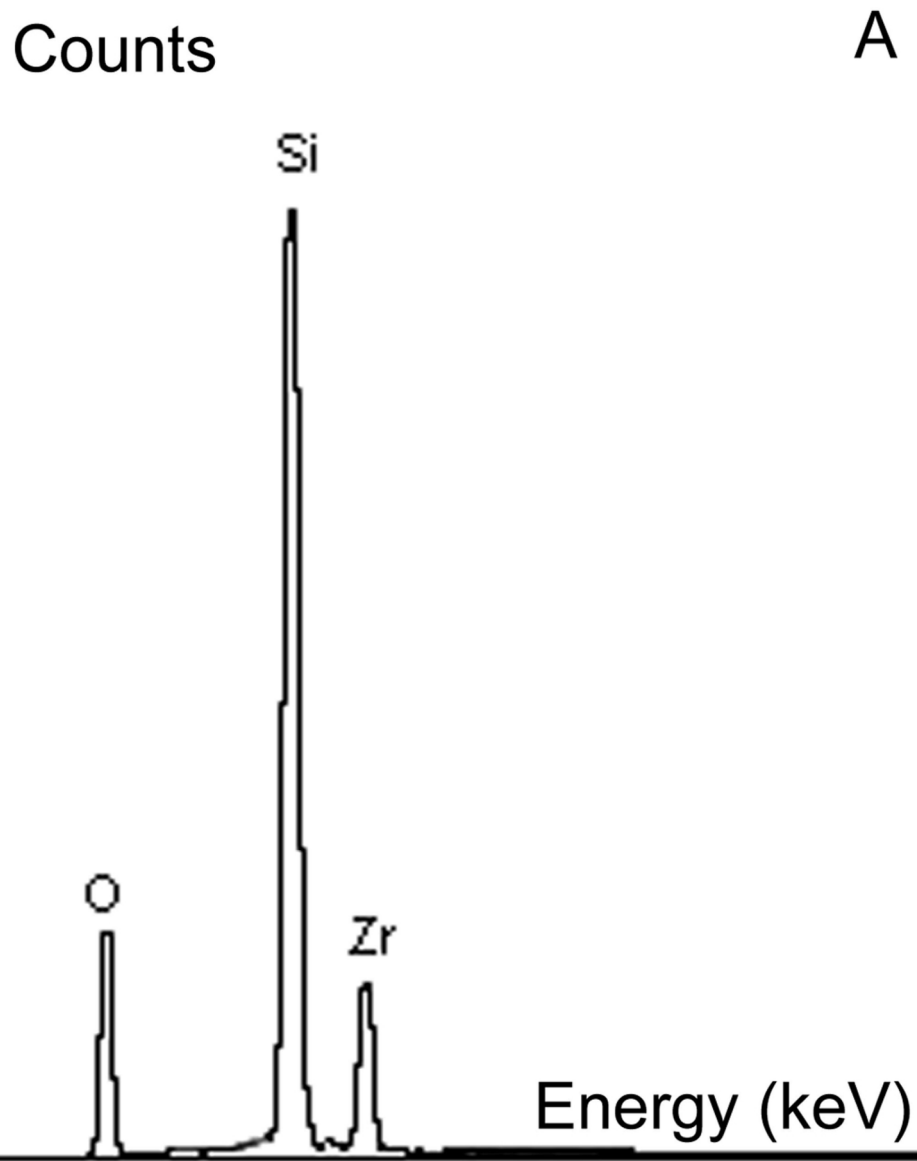Figure 14
85x78mm (300 x 300 DPI)

Figure 15 – EDS spectra of Figure 13: (a) crystals (black circles of Figure 13) (b) glassy phase
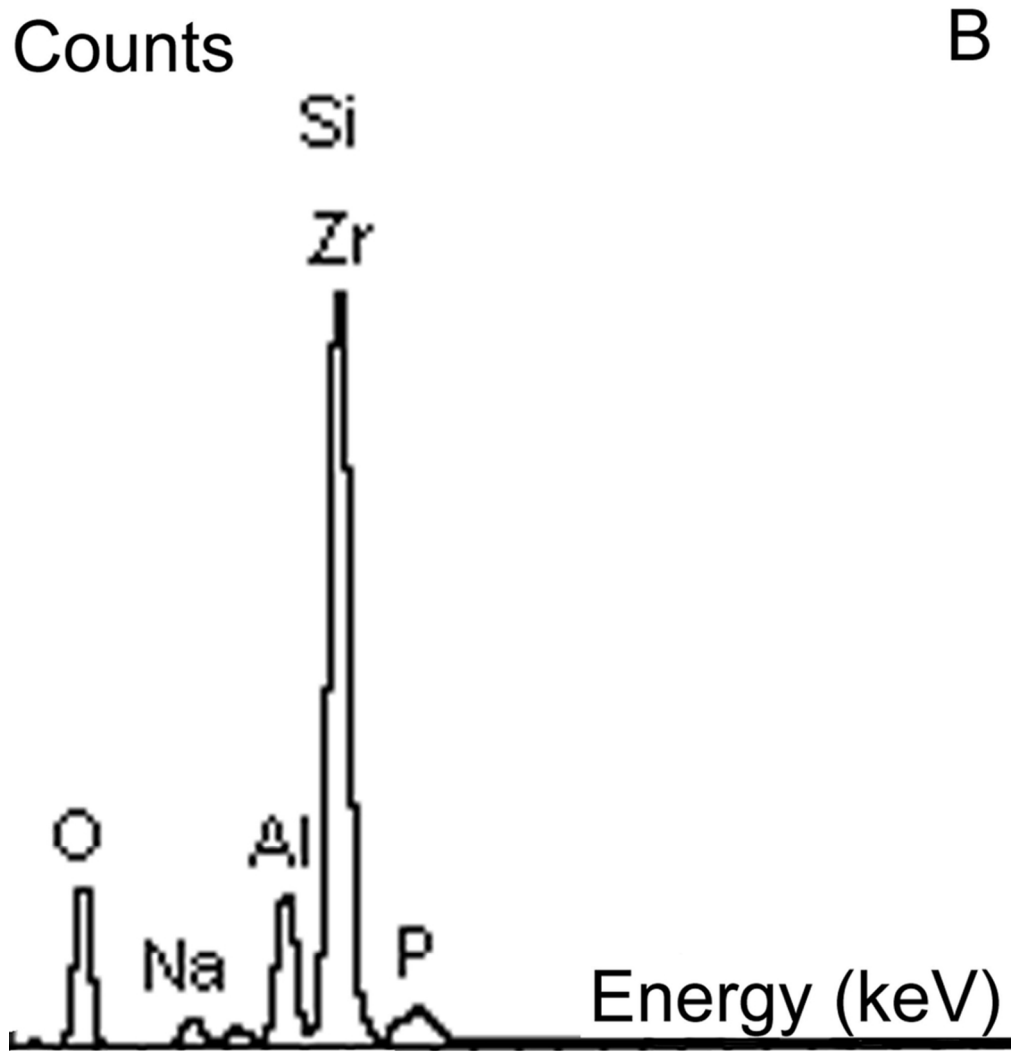Figure 15
110x144mm (300 x 300 DPI)

Figure 15 – EDS spectra of Figure 13: (a) crystals (black circles of Figure 13) (b) glassy phase
Figure 15
90x97mm (300 x 300 DPI)